# A Co9S8 microsphere and N-doped carbon nanotube composite host material for lithium-sulfur batteries

Yakun Xi, Natarajan Angulakshm, Bingyin Zhang, Xiaohui Tian, Zhihao Tang, Pengfei Xie, George Z. Chen and Yingke Zhou.

University of Nottingham
UK | CHINA | MALAYSIA

Faculty of Science and Engineering, University of Nottingham Ningbo China, 199 Taikang East Road, Ningbo, 315100, Zhejiang, China.

First published 2020



University of Nottingham
UK | CHINA | MALAYSIA

# A $Co_9S_8$ microsphere and N-doped carbon nanotube composite host material for lithium-sulfur batteries

Yakun Xi[1, †], Natarajan Angulakshmi[1, †], Bingyin Zhang[1], Xiaohui Tian[1], Zhihao Tang[1], Pengfei Xie[1], George Z. Chen[1, 2], Yingke Zhou[1,*]

[1] The State Key Laboratory of Refractories and Metallurgy, Institute of Advanced Materials and Nanotechnology, College of Materials and Metallurgy, Wuhan University of Science and Technology, Wuhan 430081, P. R. China.

[2] Energy Engineering Research Group, Faculty of Science and Engineering, University of Nottingham Ningbo China, Ningbo 316100, P. R. China.

[†]These authors contributed equally to this work. [*] Corresponding author. E-mail: zhouyk@wust.edu.cn.

**ABSTRACT**

Lithium-sulfur batteries have emerged as extraordinarily favorable energy storage devices due to their high specific capacity and energy density, safety and low cost. Unfortunately, the wide applications of lithium-sulfur batteries are hampered by several issues, such as the low electronic conductivity and slow redox kinetics, serious volumetric expansion and polysulfide "shuttle effect". To overcome these issues, in our work, we design and synthesize a composite sulfur host material of $Co_9S_8$ microspheres and N-doped carbon nanotubes, where the metallic sulfide $Co_9S_8$ with a good conductivity enables the immobilization of the polar lithium polysulfides owing to the strong polar chemisorptive capability, and the one dimensional N-doped carbon nanotubes can provide channels for fast electron and lithium-ion transport. As the lithium polysulfides are well confined, and the redox conversions are promoted, the $Co_9S_8$@N-CNTs/S-based lithium-sulfur battery possesses a superior energy storage performance, exhibiting a large specific capacity of 1233 mAh $g^{-1}$ at 0.1 C and an outstanding cyclic performance, with a low decay of 0.045% per cycle and a Coulombic efficiency of more than 99% after 1000 cycles.

**Keywords:** Metal sulfides; N-doped carbon nanotube; Cathode material; Lithium-sulfur battery.

## Graphical Abstract

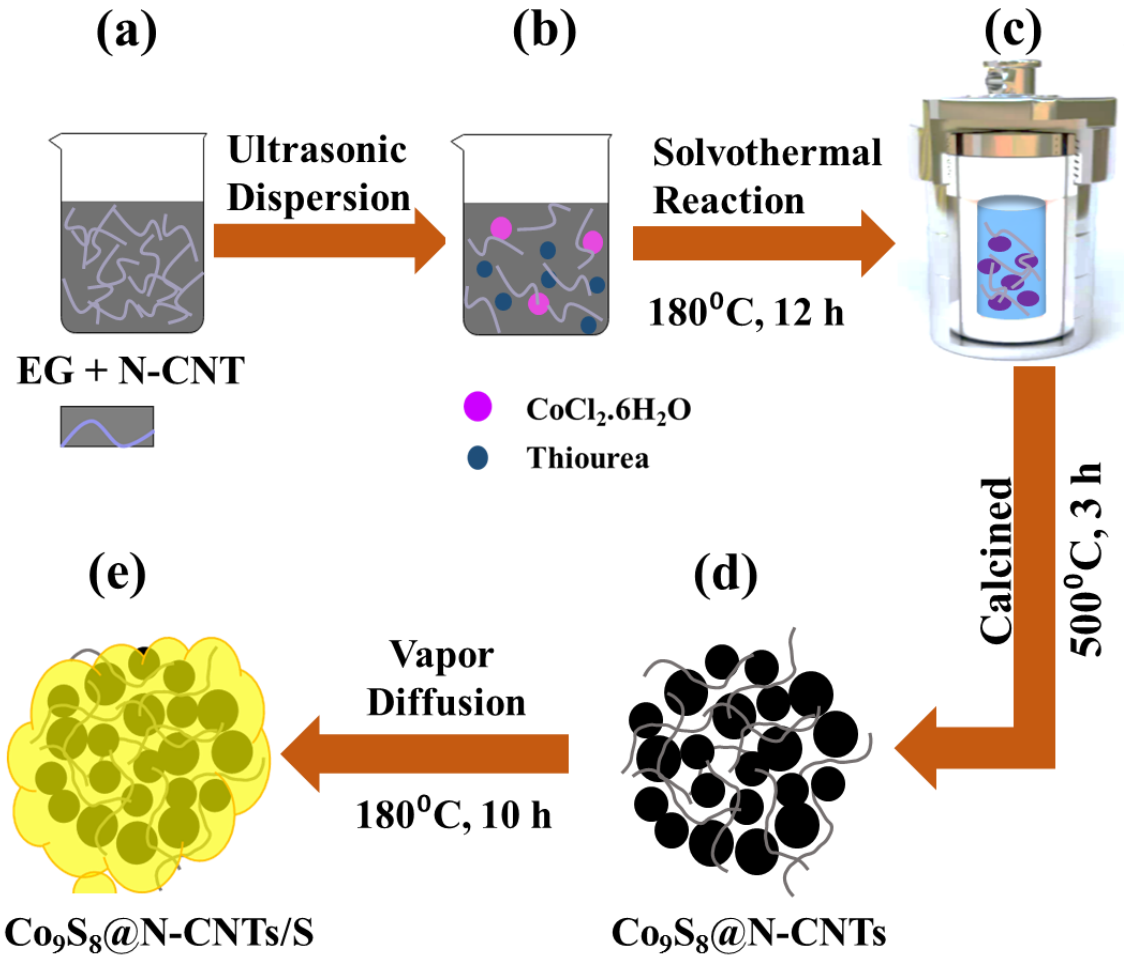

## 1. Introduction

The increase in the energy consumption and global warming has accelerated research on electrochemical energy storage devices for electric vehicles and electronic equipment [1-6]. Lithium-sulfur batteries are promising energy storage devices due to their high theoretical energy density (2600 Wh/kg) and specific capacity, natural abundance, low cost, and safety [7-11]. Unfortunately, there are some essential challenges hindering their wide applications, including the insulating nature of sulfur, the large volume change that occurs during cycling, and the dissolution and shuttling behaviors of the intermediate polysulfides, which result in poor sulfur utilization and fast capacity fading [12-15].

To overcome the abovementioned issues, researchers have adopted different strategies to construct sulfur host materials and improve the cathode performance. Various carbon nanostructures, for instance porous carbon [16], carbon nanofibers and nanotubes [17, 18] and graphene [19-30], have been used as the sulfur matrix via physical confinement. However, as nonpolar carbon materials weakly interact with sulfur, some soluble lithium sulfides may migrate from the cathode to the anode and result in decreased active material utilization and low electrode performance. Recently, some polar compounds, such as $TiO_2$ [31], $Ti_4O_7$ [32], $MnO_2$ [33], $V_2O_5$ [34], $NiS_2$ [35] and $SnS_2$ [36], have been explored to effectively confine the intermediate polysulfides by the strong chemical affinity/adsorption of polysulfides. Nevertheless, most of the polar compounds possess a poor conductivity, leading to sluggish interface redox reaction kinetics and reduced rate performances. Therefore, combining the polar compound with nanocarbon to form a host material capable of strong adsorption and with a high conductivity is beneficial to increase the conductivity, improve the electrolyte contact and provide more effective chemical and physical confinements for polysulfides, which will greatly increase the performance of lithium-sulfur batteries [37, 38].

Recently, polar $Co_9S_8$ has been proven to provide strong chemical adsorption to confine

polysulfides and possess a high catalytic activity to accelerate redox reactions and polysulfide conversion [39]. For example, $Co_9S_8$ nanotube-based cathodes demonstrate a stable cycle life and a high discharge capacity for lithium-sulfur batteries due to the enhanced conduction of electrons and Li ions and inhibition of polysulfides [40, 41]. In addition, heterojunctions based on $Co_9S_8$ and hybrids of $Co_9S_8$ and nanocarbon materials (e.g., CNTs, carbon nanofibers, hollow carbon spheres, etc.) display remarkable electrochemical performances for lithium-sulfur batteries due to the well-defined interfaces, the cooperative chemisorption of polysulfides and the synergistic dual-confinement effects [42-46]. Compared to pristine CNT, doping CNTs with N can enhance their electronic conductivity, as more electron carriers are provided by the dopants in the conduction band. The introduced nitrogen-containing functional groups can increase the surface polarity, and the defects and nonuniformities in the N-CNTs may serve as active sites for the adsorption of S and polysulfides and the deposition of $Li_2S$. Moreover, the N-CNT networks may also tightly connect and confine the sulfur substances to enhance the structural integrity of the composite electrode and serve as the steady "highways" to accelerate electron transport [47, 48]. In this work, the composite of $Co_9S_8$ microspheres and N-CNTs was synthesized by a facile solvothermal method and subsequent annealing. The synthesis process is convenient, and a three-dimensionally interconnected network structure with the $Co_9S_8$ microspheres tightly attached to the N-CNTs is formed. In this composite, the polar metal sulfide $Co_9S_8$ enables a superior lithium polysulfide absorptivity via the polar chemical bond, which decreases polysulfide dissolution and the shuttle effect and increases the specific capacity and cyclic performance, while the N-doped carbon nanotubes can assist to increase the electronic conductivity and enlarge the interface between the electrode and electrolyte to further enhance the rate performance. Meanwhile, the N-CNTs/S composite and the $Co_9S_8$@N-CNTs/S composites with different contents of N-CNTs have been studied and compared. The unique $Co_9S_8$@N-CNTs composite-based sulfur cathode displays an outstanding overall electrochemical performance, making it promising for applications in

lithium-sulfur batteries.

## 2. Experimental

### *2.1 Preparation of $Co_9S_8$ and $Co_9S_8$@N-CNTs*

The $Co_9S_8$@N-CNTs composite host was prepared using a solvothermal process. First, 27 mg of the N-CNTs was ultrasonically dispersed into 30 mL of ethylene glycol and 10 mL of distilled water to form a suspension. $CoCl_2 \cdot 6H_2O$ (0.7138 g) and thiourea (0.4567 g) were added with stirring, and the ratio of $CoCl_2$:thiourea was fixed as 60:40. The obtained solution was then subjected to a hydrothermal reaction for 12 h at 180 °C. The product was filtered, adequately washed, and vacuum-dried for 24 h at 80 °C. The obtained precursor was annealed for 3 h at 500 °C in $H_2$/Ar (10%:90%). The obtained sample is denoted as $Co_9S_8$@N-CNTs. The pristine $Co_9S_8$ material was also prepared using the same processes but without adding the N-CNTs. The other $Co_9S_8$@N-CNTs composites with different contents of N-CNTs (13.5 mg and 40.5 mg) were prepared by a similar procedure. Hereafter, these obtained samples with different N-CNT contents are denoted as $Co_9S_8$@N-CNTs-1 and $Co_9S_8$@N-CNTs-2.

### *2.2 Synthesis of S-impregnated materials*

Sulfur is loaded by a vapor diffusion method. The S-impregnated materials were obtained by mixing both sublimed sulfur and the $Co_9S_8$@N-CNTs (1:4) in a Teflon-lined stainless steel autoclave filled with Ar, which was subsequently heating for 10 h at 180 °C. For comparison, either pristine $Co_9S_8$ or the N-CNTs was also loaded with sulfur using the same procedure to obtain the composites.

### *2.3 Characterization*

The powder X-ray diffraction (XRD) analysis was performed with an X-pert Pro MPD diffractometer. The morphology and structure were observed using scanning electron microscopy (SEM, PHILIPS-XL30TMP) and transmission electron microscopy (TEM, FEI

Tecnai-G20, 200 kV). A VG Multilab 2000 apparatus was used to perform X-ray photoelectron spectroscopy (XPS), thermogravimetric analysis (STA449/6/G, NETZSCH) was performed to determine the carbon and sulfur contents, and a Shimadzu UV3600 instrument was used to obtain the ultraviolet-visible absorption spectra.

2.4 Electrochemical measurements

The cathode slurry comprising 70 wt% of the synthesized materials, 20 wt% of Super-P, and 10% of PVDF was made by mixing in NMP and coated onto an Al film before vacuum drying for 24 h at 60 °C. The separator was a Celgard 2400 polypropylene membrane, the counter electrode was a Li foil, and the electrolyte was 1 M LiTFSI + 0.1 M $LiNO_3$ dissolved in dimethoxyethane and 1,3-dioxolane (1:1). The coin cells (2032 type) were assembled in a glove box filled with argon. A Neware battery test system (5V5mA) was used to obtain the charge/discharge profiles at various rates within 1.7-2.8 V and the capacities were calculated based on the mass of sulfur. A CHI 660D electrochemical workstation was used to obtain the cyclic voltammetry (CV) curves within 1.7-2.8 V and the electrochemical impedance spectroscopy (EIS) between 10 mHz~1 MHz.

*2.5 $Li_2S_6$ adsorption capability*

Sulfur powder and $Li_2S$ (5:1) were dissolved in dimethoxyethane and 1,3-dioxolane (1:1) and stirred for 48 h at 80 °C to form the $Li_2S_6$ solution. Then, 30 mg of $Co_9S_8$, N-CNTs or the $Co_9S_8$@N-CNTs were separately added to the obtained $Li_2S_6$ solution (5 mL) to investigate the absorption ability of the polysulfides.

**3. Results and discussion**

The preparation of the $Co_9S_8$@N-CNTs microspheres and $Co_9S_8$@N-CNTs/S composite is illustrated in Fig. 1. The $Co_9S_8$ microsphere precursor with interconnected N-CNTs was first prepared by a solvothermal process, during which the $Co^{2+}$ ions would be absorbed on the surface of the N-CNTs to form uniformly distributed $Co_9S_8$ due to the electrostatic

attraction effect [34]. After annealing in a reducing atmosphere, the $Co_9S_8$@N-CNTs were successfully obtained. Finally, a vapor diffusion process was used to load sulfur and form the $Co_9S_8$@N-CNTs/S composite. The morphology and structure of the as-synthesized materials were observed by SEM, as shown in Fig. 2(a-d). Fig. 2(a) shows that the $Co_9S_8$ microspheres (approximately 3~8 μm) are mainly composed of secondary nanoparticles with sizes of approximately 10 nm. Fig. 2(b) shows the SEM image of the $Co_9S_8$@N-CNTs, showing that the N-CNTs (11.2%, as shown in Fig. S1) spread throughout and interconnect with the monodisperse $Co_9S_8$ microspheres. Such a 3D network structure is favorable to transport electrons and ions. After loading with sulfur, some agglomerations of melted sulfur and the $Co_9S_8$ microspheres are observed for the pristine $Co_9S_8$ material (Fig. 2(c)), while the structure and morphology of the $Co_9S_8$@N-CNTs are basically retained, and sulfur is homogeneously deposited, as shown in Fig. 2(d). The TEM image (Fig. 3(a)) and the EDX elemental mapping image of the $Co_9S_8$ microspheres (Fig. 3(b) and (c)) exhibit the homogenous distribution of Co and sulfur elements. Fig. 3(d) shows the high-resolution TEM image, where the lattice distance is 0.3 nm and corresponds to the (311) plane of $Co_9S_8$, implying the high crystallinity of the $Co_9S_8$ material [35].

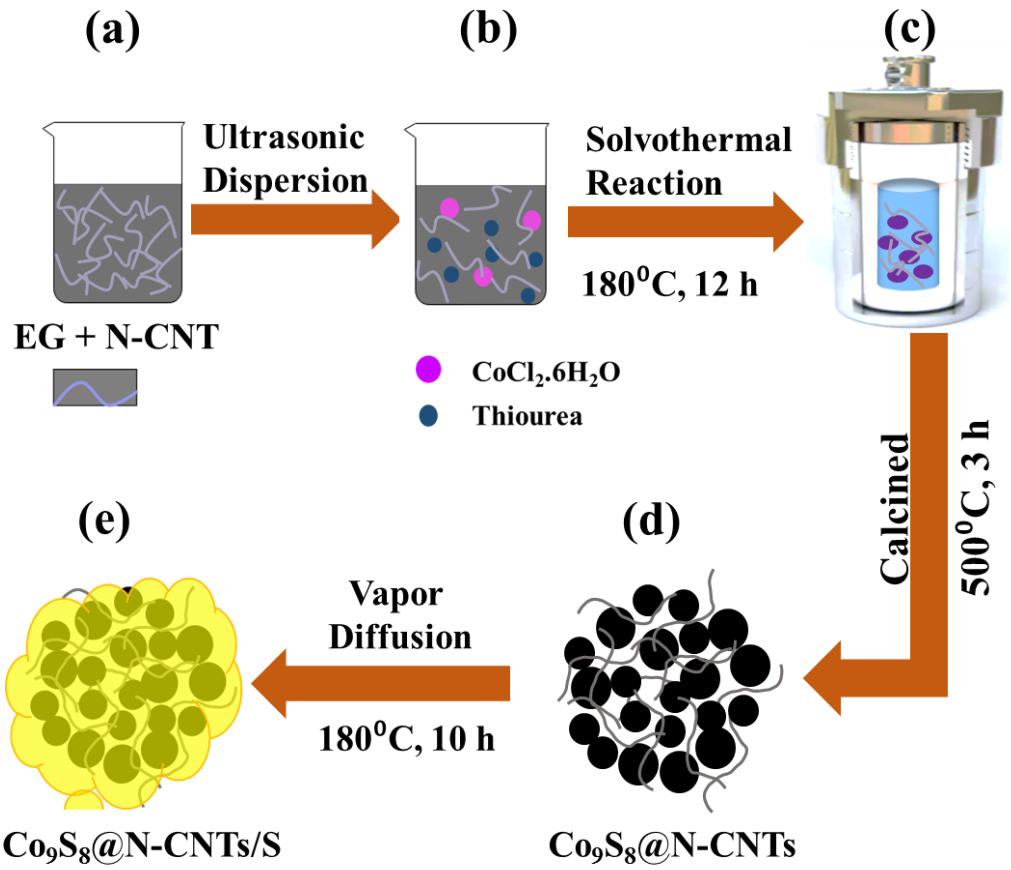


**Fig. 1** Schematics of the synthesis of the $Co_9S_8$@N-CNTs/S: (a) dispersion of the N-CNTs in an ethylene glycol (EG) solution, (b) precursor of $Co_9S_8$ with the N-CNTs, (c) solvothermal reaction performed at 180 °C for 12 h, (d) calcination of the $Co_9S_8$@N-CNT composite at 500°C for 3 h, and (e) impregnation of sulfur on the $Co_9S_8$@N-CNT composite ($Co_9S_8$@N-CNT/S).

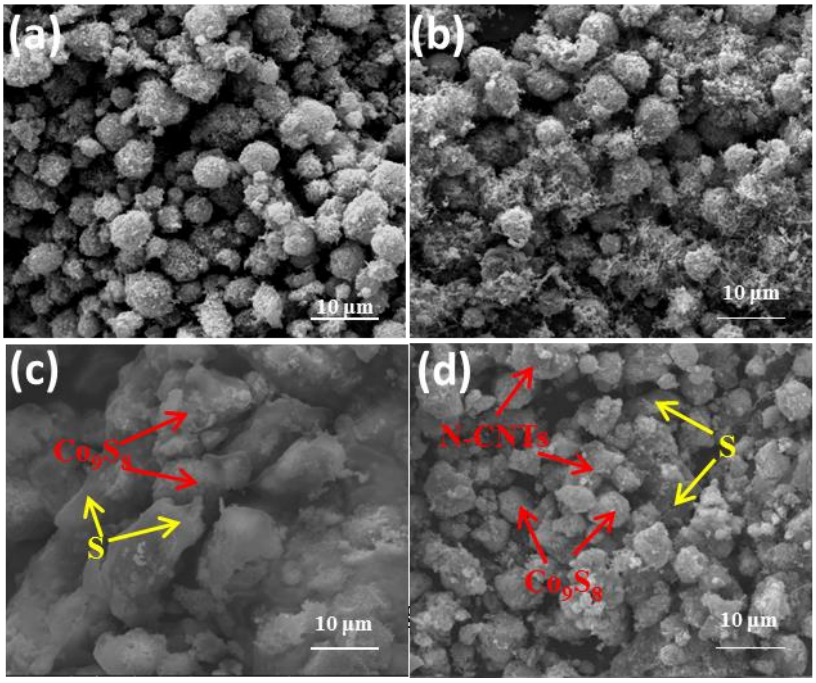


**Fig. 2** SEM images of $Co_9S_8$ (a), $Co_9S_8$@N-CNTs (b), $Co_9S_8$/S (c) and $Co_9S_8$@N-CNTs/S (d).

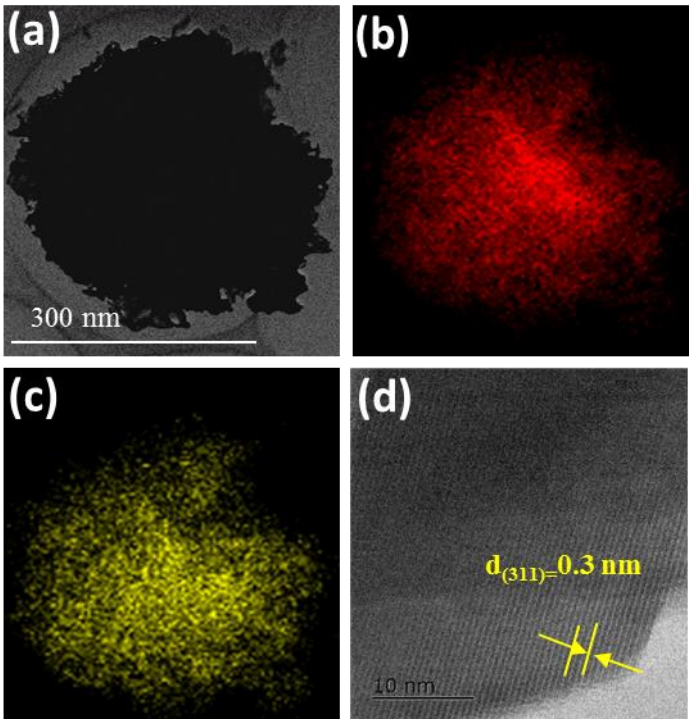


**Fig. 3** TEM image of $Co_9S_8$ (a), EDX image of Co (b) and S (c), and HRTEM image of $Co_9S_8$ (d).

Fig. 4 shows the XRD patterns of the materials. As shown in Fig. 4(a), the diffraction peak of the N-CNTs at 26.1° is attributed to the graphitic carbon. All the diffraction peaks of $Co_9S_8$ and $Co_9S_8$@N-CNTs are assignable to cubic *Fm-3m* $Co_9S_8$ (JCPDS card no. 19-0364) [36], indicating the good crystallinity of both materials and the negligible effect of the N-CNTs on the $Co_9S_8$ structure. As the percentage of the N-CNTs is relatively low (～11.2%), the peak corresponding to the N-CNTs at approximately 26° might be shielded/overlapped by the stronger diffraction peak of $Co_9S_8$. Therefore, the peak corresponding to the N-CNTs was not observed for the $Co_9S_8$@N-CNTs sample. As shown in Fig. 4(b), the strong orthorhombic peaks for sulfur are observed in the XRD patterns of $Co_9S_8$/S and the $Co_9S_8$@N-CNTs/S (JCPDS card No.08−0247), indicating that sulfur has been successfully incorporated, and the good crystallinity is probably due to the vapor diffusion process (180 °C, 10 h) used to load sulfur [37]. The XRD peaks of $Co_9S_8$ in the composites after loading sulfur are not evident, probably because of the shielding/overlapping effects induced by the relatively high sulfur loading (～70%). Fig. 5 displays the TGA profiles of the sulfur, N-CNT/S, $Co_9S_8$/S, $Co_9S_8$@N-CNTs/S, $Co_9S_8$@N-CNTs-1/S and $Co_9S_8$@N-CNTs-2/S composites. The weight loss of all the samples ends at approximately 350 °C. The sulfur content is ～70% for $Co_9S_8$/S and ～75% for all of the $Co_9S_8$@N-CNTs/S composites. The higher sulfur ratio of the $Co_9S_8$@N-CNTs/S composites may result from the penetration of sulfur inside the N-CNTs from the $Co_9S_8$@N-CNTs composite network, which is consistent with the SEM results.

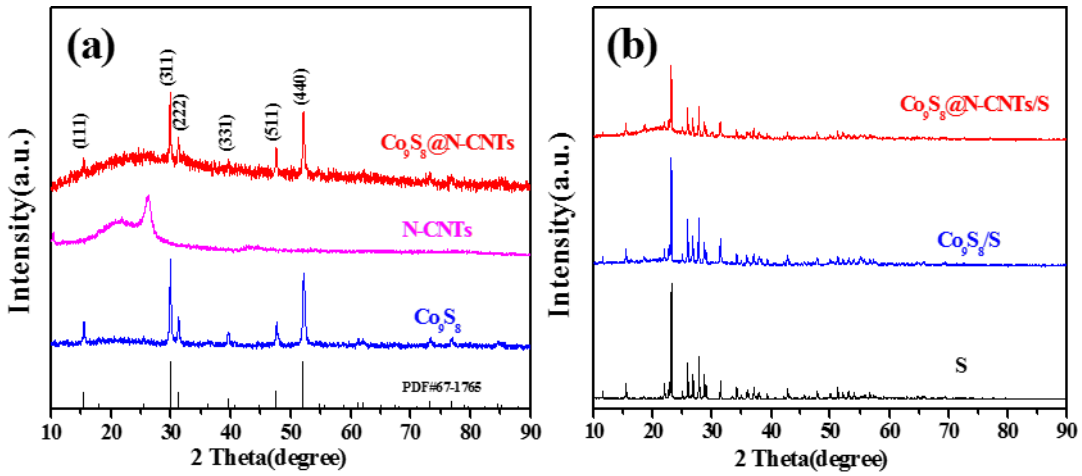


**Fig. 4** XRD patterns of (a) $Co_9S_8$, N-CNTs and the $Co_9S_8$@N-CNT composite and (b) sulfur, $Co_9S_8$/S, and the $Co_9S_8$@N-CNT/S.

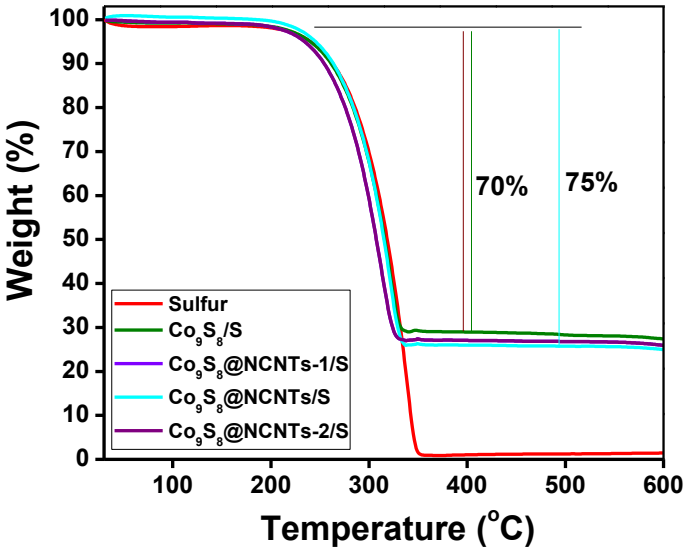


**Fig. 5** TGA profiles of sulfur, $Co_9S_8$/S, $Co_9S_8$@N-CNTs-1/S, $Co_9S_8$@N-CNTs/S and $Co_9S_8$@N-CNTs-2/S.

To compare the polysulfide absorptivity, the $Co_9S_8$, N-CNTs and $Co_9S_8$@N-CNTs materials were separately put into a $Li_2S_6$ solution. As displayed in Fig. 6(a) and Fig. S3, at the beginning, all of the solutions are the same yellow color. The yellow solution obtained with

the addition of the $Co_9S_8$@N-CNTs turns colorless after 1 hour, indicating the strong chemisorption between $Li_2S_6$ and the $Co_9S_8$@N-CNTs [49]. In contrast, the solutions obtained with the addition of $Co_9S_8$ or the N-CNTs still display slight yellow colors. Fig. 6(b) shows the UV-vis absorption spectra obtained for the $Li_2S_6$ solutions without or with the addition of $Co_9S_8$ and the $Co_9S_8$@N-CNTs. The $Li_2S_6$ solution shows an obvious polysulfide absorption peak at approximately 411 nm, while both peaks are negligible for the $Li_2S_6$ solution soaked with $Co_9S_8$ and the $Co_9S_8$@N-CNTs. Moreover, the peak intensity of the $Co_9S_8$@N-CNTs is weaker than that of $Co_9S_8$, implying the stronger absorption ability of the $Co_9S_8$@N-CNTs composite, which may effectively suppress the dissolution and shuttling effect of polysulfide during cycling [50]. The XPS survey spectrum of the $Co_9S_8$@N-CNTs composite was recorded and shown in Fig. 7(a), where the distinct peaks corresponding to Co 2p, S 2p, C 1s, N 1s and O 1s are observed. The Co $2p_{3/2}$ spectrum shown in Fig. 7(b) is decomposed into five peaks in the range of 771-789 eV, which not only indicates the presence of $Co^{3+}$ and $Co^{2+}$ at binding energies of approximately 778.4 eV and 781.9 eV, corresponding to the cobalt ion in the octahedron and tetrahedron sites in $Co_9S_8$ [51-55], but also includes two additional peaks at 780.56 eV and 783.2 eV, corresponding to the Co-S and Co-N bonds. Fig. 5(c) shows that the S 2p spectrum is decomposed into six peaks. The S $2p_{3/2}$ and S $2p_{1/2}$ components at 162.4 eV and 163.4 eV suggest the existence of S-S species [35]. In addition, the other three peaks appearing at 161.5 eV, 164.4 eV and 166.5 eV correspond to the Co-S, C-S and S-N bonds. The $SO_4^{2-}$ component may be caused by the slight oxidation of the sample surface. The spectrum of C 1s shown in Fig. 7(d) includes three main peaks at binding energies of 284.2, 284.6 and 285.5 eV, corresponding to C-S, the $sp^2$ carbon of C=C, and C-N, respectively [56-58], confirming the incorporation of the N-CNTs and the interaction between $Co_9S_8$ and the N-CNTs. The N 1s spectrum shown in Fig. 7(e) can be fitted by four components at 402.0, 400.6, 399.6, and 398.4 eV, which are attributed to graphitic N, pyrrolic N, amine N and pyridinic N, respectively. Due to the unique crystal and electronic structure of $Co_9S_8$, there

might be a strong chemical interaction between $Co_9S_8$ and the polysulfides, as the Li atoms in polysulfides can form bonds with the S on the $Co_9S_8$ surfaces, and the S in the polysulfides can also form bonds with the Co on the $Co_9S_8$ surfaces because of the anion-cation Coulomb interactions. In addition, the introduced nitrogen-containing functional groups can increase the surface polarity of the CNTs, which is beneficial to further increasing the adsorption and confinement of lithium polysulfides. Therefore, the polar surface and the various chemical states of the composite may contribute to the strong interactions and adsorption of lithium polysulfides [59].

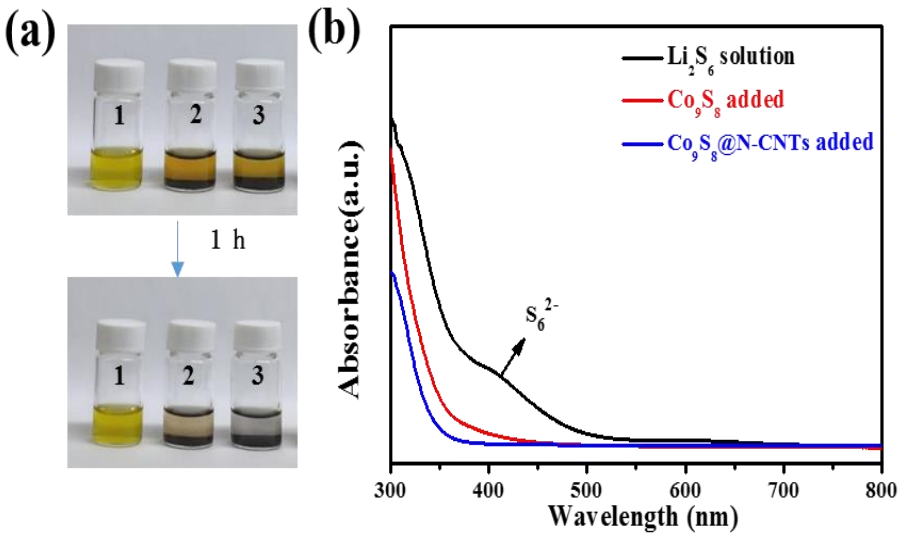


**Fig. 6** Optical photographs showing the color change of the $Li_2S_6$ solution after adding $Co_9S_8$ and $Co_9S_8$@N-CNTs: (1) $Li_2S_6$ solution, (2) $Li_2S_6$ solution with added $Co_9S_8$, and (3) $Li_2S_6$ solution with the added $Co_9S_8$@N-CNTs (a). UV-vis absorption spectra collected for the $Li_2S_6$ solution soaked with $Co_9S_8$ and the $Co_9S_8$@N-CNTs (b).

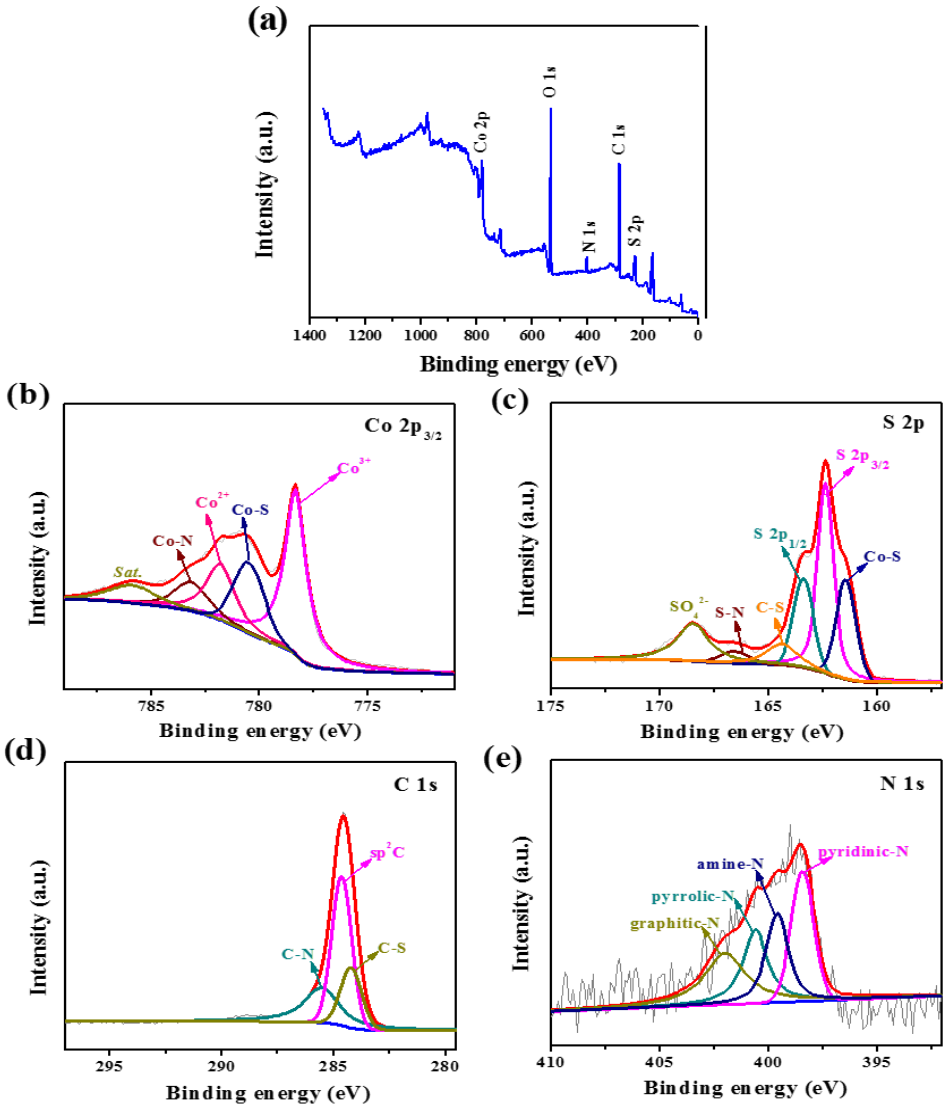


**Fig. 7** XPS survey spectrum of $Co_9S_8$@N-CNTs (a), core level XPS spectra of Co $2p_{3/2}$ (b), S 2p (c), C 1s (d) and N 1s (e) of $Co_9S_8$@N-CNTs.

To evaluate the performances of the $Co_9S_8$@N-CNTs/S composite material, coin cells with the $Co_9S_8$@N-CNTs/S cathodes and Li anodes were assembled and compared to the $Co_9S_8$/S cathode. Fig. 8(a) exhibits the initial charge-discharge profiles obtained for $Co_9S_8$/S and the $Co_9S_8$@N-CNTs/S at 0.1 C. The specific discharge capacities of the $Co_9S_8$@N-CNTs/S and $Co_9S_8$/S are 1233 and 1016 mAh $g^{-1}$, respectively, indicating that the

nitrogen-doped carbon nanotube network can efficiently improve the specific capacity. The rate performance of the cathodes was observed at various current rates of 0.1-2 C (Fig. 8(b)). The $Co_9S_8$/S material exhibits specific discharge capacities of 1016, 826, 689, 635 and 543 mAh $g^{-1}$ at 0.1, 0.2, 0.5, 1 and 2 C, respectively. In contrast, the specific discharge capacities of the $Co_9S_8$@N-CNTs/S at 0.1 0.2, 0.5, 1 and 2 C are 1233, 1066, 925, 841 and 713 mAh $g^{-1}$, respectively, which are higher than those of $Co_9S_8$/S. When switched back to 0.1 C, more than 88% of the original capacities were recovered for the $Co_9S_8$@N-CNTs/S cells (Fig. 8(b)), indicating the fast reaction kinetics of the $Co_9S_8$@N-CNTs/S electrode. The superior rate capability of the $Co_9S_8$@N-CNTs/S may result from the accelerated ion transport and electron transfer from the three dimensional N-CNT and $Co_9S_8$ composite network structure.

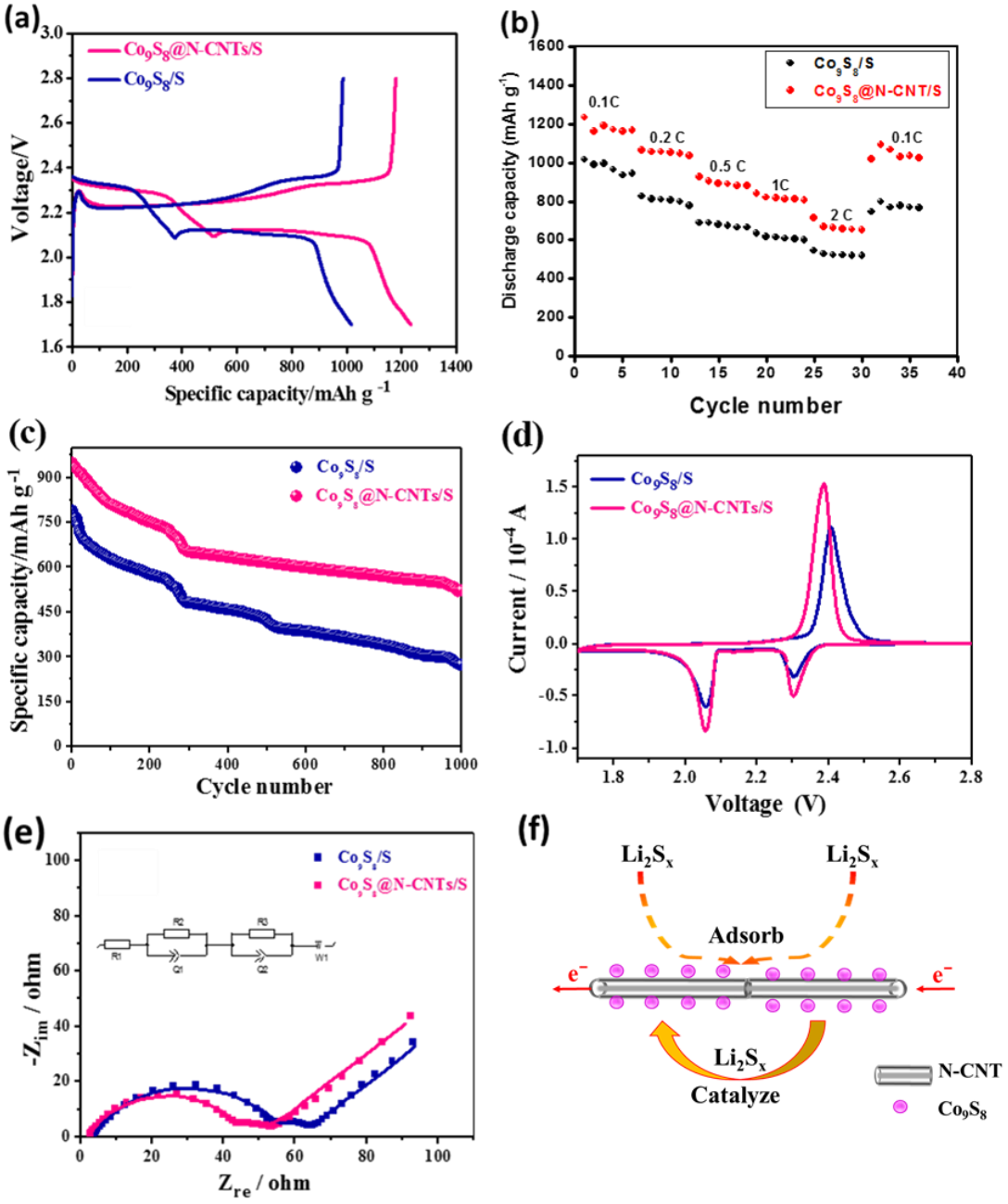


**Fig. 8** Discharge/charge curves (0.1 C) (a), rate performances (b), cyclic performance (0.5 C) (c), CV profiles (d), and EIS plots (e) of the $Co_9S_8$/S and $Co_9S_8$@N-CNTs/S cathodes respectively, and depiction of the accelerated polysulfide adsorption and conversion of $Co_9S_8$@N-CNTs (f).

The $Co_9S_8$/S and $Co_9S_8$@N-CNTs/S cathodes were cycled for 1000 cycles at 0.5 C to study their cyclic performance, and the results are shown in Fig. 8(c). The $Co_9S_8$@N-CNTs/S electrode initially exhibits a capacity of ~950 mAh $g^{-1}$, which is higher than the capacity of $Co_9S_8$/S, 788 mAh $g^{-1}$. After 300 cycles, the capacities of 652 and 480 mAh $g^{-1}$ were retained for the $Co_9S_8$@N-CNTs/S and $Co_9S_8$/S, respectively, which corresponds to a retention of 68.63% and 60.91% at the end of 300 cycles. After 1000 cycles, the $Co_9S_8$@N-CNTs/S cathode still maintains the specific capacity of 522 mAh $g^{-1}$, the Coulombic efficiency is higher than 99%, and the average decay is approximately 0.045% for one cycle [60]. In contrast, the $Co_9S_8$/S cathode exhibits a much lower discharge capacity (273 mAh $g^{-1}$), higher decay (0.065% after one cycle) and lower Coulombic efficiency (97%). As shown in Fig. 8(c), during the long-term cycling at 0.5 C, both of the synthesized samples experienced a rapid decay and a less rapid decay. There are some mono-dispersed $Co_9S_8$ microspheres/sulfur in the composite, which may suffer from volume expansion and sulfur dissolution during the continuous charging-discharging and cause fast capacity decay during the first 300 cycles. However, the decay that occurred for the $Co_9S_8$@N-CNTs/S composite is relatively slow compared to that of the $Co_9S_8$/S composite after 300 cycles, which is probably because the stronger chemical interaction between the polysulfides and the former effectively inhibited the “shuttle effect” and reduced the capacity decay. Meanwhile, an N-CNTs/S cathode was also evaluated and delivered a discharge capacity of 500 mAh $g^{-1}$ in the first cycle, after which the capacities were gradually reduced to 100 mAh $g^{-1}$ in the $1000^{th}$ cycle performed at 0.5 C, which is a worse cycling performance compared to that of the $Co_9S_8$@N-CNTs/S composite, as shown in Fig. S4. The increased performance of the $Co_9S_8$@N-CNTs/S may result from the strong chemical interaction and binding between the $Co_9S_8$ and N-CNT composite and polysulfides, which can effectively suppress the dissolution and shuttling effect of polysulfide during cycling. To investigate the structure stability, additional SEM images of the $Co_9S_8$@N-CNTs/S electrode were obtained before and after cycling, as shown in Fig.

S5(a) and (b). Fig. S5(b) demonstrates that the active material in the cycled electrode basically retains the morphology of the initial composite before cycling (Fig. S5(a)), indicating the good structure stability during high current density cycling. Compared to the XPS spectra of the $Co_9S_8$@N-CNTs/S electrode in the charge state, a new peak at 164 eV was observed in the discharged state, as shown in Fig. S7, which is attributed to the Li-S bond and indicates the formation of the new Li-S bond after the discharging process. These results indicate that the lithium polysulfides are firmly confined on the electrode surface and further confirm the interaction between the cathodes and lithium polysulfides. Compared to other reported sulfur cathodes based on metal oxides and sulfides, as listed in Table S1, the $Co_9S_8$@N-CNTs/S cathode shows a relatively higher rate capability and cycling performances [61-66].

The lithium storage performances of the $Co_9S_8$@N-CNTs/S composite cathodes with different contents of N-CNTs (8.8% for N-CNTs-1 and 14.9% for N-CNTs-2, as shown in Fig. S1) were measured, and the results are shown in Fig. S6. The N-CNTs-1 and N-CNTs-2 cells delivered discharge capacities of approximately 385 and 400 mAh $g^{-1}$ at 0.5 C, respectively, which are lower compared to of the $Co_9S_8$@N-CNTs/S composite cathode at the same rate. Fig. 8(d) displays the CV curves of the $Co_9S_8$/S and $Co_9S_8$@N-CNTs/S electrodes within 1.7-2.8 V at 0.1 mV/s. Both curves show one oxidation peak and two reduction peaks. During the cathodic scanning process, the first peak is associated with the reduction of cyclic $S_8$ molecules to long chain polysulfides ($Li_2S_n$, $4 \leq n \leq 8$), and the second peak is related to the transformation of the long $Li_2S_n$ chain to the short $Li_2S_2$/$Li_2S$ chain [67]. During the anodic scanning process, the anodic peak is ascribed to the transformation of $Li_2S_2$/$Li_2S$ back to $S_8$. Both reduction peaks at approximately 2.30 and 2.05 V appear for the $Co_9S_8$/S and $Co_9S_8$@N-CNTs/S electrodes, but the peaks of the $Co_9S_8$@N-CNTs/S are sharper and have a higher intensity than those of the $Co_9S_8$/S electrodes. In addition, the anodic peaks appear at 2.40 V and 2.38 V for $Co_9S_8$/S and $Co_9S_8$@N-CNTs/S, respectively. The oxidation peak of the $Co_9S_8$@N-CNTs/S electrode is

also sharper, has a higher intensity and is negatively shifted compared to that of $Co_9S_8$/S, indicating the higher reversibility of the $Co_9S_8$@N-CNTs/S cathode.

Fig. 8 (e) shows the Nyquist plots obtained for the $Co_9S_8$/S and $Co_9S_8$@N-CNTs/S cathodes. Both plots show a high-frequency semicircle, a medium-frequency semicircle and a low-frequency inclined line, which correspond to the solid interface layer of the electrode surface, the charge-transfer process, and the Warburg impedance within the cathode, respectively [68]. The charge-transfer resistance of the $Co_9S_8$@N-CNTs/S cathode is approximately 53 Ω, which is much lower compared to that of $Co_9S_8$/S (64 Ω). These results imply that the $Co_9S_8$@N-CNTs/S electrode exhibits increased ion and charge transfer rates and higher material utilization than $Co_9S_8$/S, which may contribute to the improved energy storage performance of the $Co_9S_8$@N-CNTs/S [69-74].

The outstanding lithium storage characteristics of the $Co_9S_8$@N-CNTs/S may be ascribed to the unique composite structure and properties. As shown in Fig. 8(f), the $Co_9S_8$/N-CNTs composite possesses an open and porous three-dimensional structure, which provides sufficient space for electrolyte penetration and an adequate interface for Li-ion transport [75]. Both the $Co_9S_8$ microspheres and N-CNTs can immobilize polysulfides by chemical bonds to suppress polysulfide dissolution and thus increase the sulfur utilization. Specifically, the polysulfides can be strongly adsorbed on the $Co_9S_8$ surfaces due to the coexistence of Co−S and Li−S bonds, which results in electron transfer from the polysulfides to the Co atoms and accelerates the reaction kinetics of the polysulfides decomposing to the final insoluble products on $Co_9S_8$, and the electrochemical reaction kinetics could be greatly increased during the discharge/charge processes occurring in Li–S batteries [52, 53]. In addition, the N-CNTs not only promote the electronic conductivity but also buffer the volume expansion of elemental sulfur. Therefore, a remarkable increase in the discharge capacity, rate performance and cyclic stability of the lithium-sulfur battery is achieved [76].

To explore the contribution of the spherical metal sulfide $Co_9S_8$ to the capacity of the composites, the lithium storage behaviors of the $Co_9S_8$ microsphere (without impregnation of sublimed sulfur) and the N-CNTs (without impregnation of sublimed sulfur) were measured within 1.7–2.8 V, as shown in Fig. 9 and Fig. S8. The pristine $Co_9S_8$ and N-CNTs cathodes display a low initial specific capacity of 23 and 26 mAh $g^{-1}$, and retain capacities of 9.6 and 7 mAh $g^{-1}$ after 200 cycles at 0.2 C, respectively, suggesting the negligible contribution of $Co_9S_8$ and the N-CNTs to the capacity of the $Co_9S_8$/S and $Co_9S_8$@N-CNTs/S composite cathodes. Therefore, the N-CNTs can promote the electronic conductivity and provide the additional adsorption and confinement of the polysulfides to prevent shuttling and synergistically increase the charge/discharge cycling performance of the S composite cathodes with $Co_9S_8$.

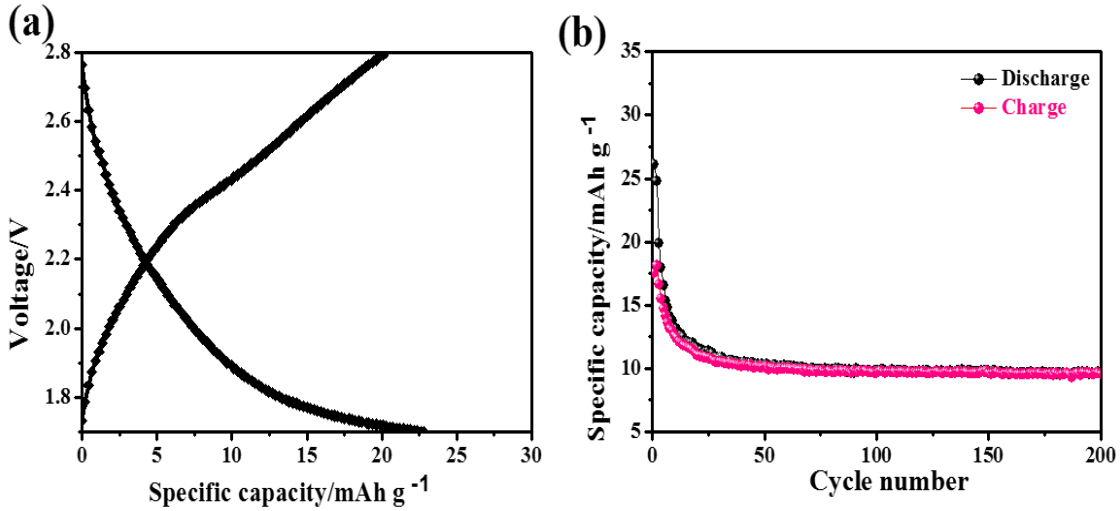


**Fig. 9** Discharge-charge profiles of the $Co_9S_8$ electrode (without the impregnation of sulfur) at 0.2 C (a), and cycling performance of the $Co_9S_8$ electrode (without the impregnation of sulfur) at 0.2 C (b).

## 4. Conclusions

A unique sulfur host material composed of $Co_9S_8$ microspheres and interlaced N-CNTs has

been designed and realized. In this novel structure, the polar chemical bond in $Co_9S_8$ can strength the confinement of the soluble lithium polysulfides and mitigate the shuttle effect, and the nitrogen-doped carbon nanotubes interconnected with the metallic sulfide enable a highly conductive network and a high specific interface for the rapid transfer of charges. As a result, the $Co_9S_8$@N-CNTs/S composite exhibits superior lithium storage characteristics of improved specific discharge capacity, outstanding cyclic and rate performance. The $Co_9S_8$@N-CNTs/S cathode displays a good cycling capability and a high Coulombic efficiency for up to 1000 cycles at 0.5 C, demonstrating that the novel composite structure is a potential sulfur host material for practical applications in lithium-sulfur batteries.

**Acknowledgements**

The authors gratefully acknowledge the National Natural Science Foundation of China (No. 51974209) and the Natural Science Foundation of Hubei Province of China (No. 2013CFA021, 2018CFA022).

**References**

[1] R. Schmuch, R. Wagner, G. Horpel, T. Placke, M. Winter, Performance and cost of materials for lithium-based rechargeable automotive batteries, Nat. Energy 3 (**2018**) 267-278.

[2] Y. Zhou, J. Lu, C. Deng, H. X. Zhu, G. Z. Chen, S. W. Zhang, X. H. Tian, Nitrogen-doped graphene guided formation of monodisperse microspheres of $LiFePO_4$ nanoplates as the positive electrode material of lithium-ion batteries, J. Mater. Chem. A 4 (**2016**) 12065-12072.

[3] X. H. Tian, Y. Zhou, X. F. Tu, Z. T. Zhang, G. D. Du, Well-dispersed $LiFePO_4$ nanoparticles anchored on a three-dimensional graphene aerogel as high-performance positive electrode materials for lithium-ion batteries, J. Power Sources 340 (**2017**) 40-50.

[4] X. H. Tian, Y. Zhou, G. Wu, P. C. Wang, J. Chen, Controllable synthesis of porous $LiFePO_4$ for tunable electrochemical Li-insertion performance, Electrochim. Acta 229 (**2017**) 316-324.

[5] B. Wu, Y. Xie, Y. Meng, C. Qian, Y. Chen, A. Yuan, X. Guo, H. Yang, S. Wan, S. Lin, Constructing unique heterogeneous cobalt-manganese oxide porous microporous as anode for long-cycle and high-rate lithium ion batteries, J. Mater. Chem. A 7 (**2019**) 6149-6160.

[6] Z. Wang, Z. Zhang, J. Xia, W. Wang, S. Sun, L. Lu, H. Yang, $Fe_2O_3$@C core@shell nanotubes: porous $Fe_2O_3$ nanotubes derived from MIL-88A as cores and carbon as shells for high power lithium-ion batteries, J. Alloys Compd. 769 (**2018**) 969-976.

[7] A. Manthiram, Y. Fu, S. H. Chung, C. Zu, Y. Su, Rechargeable lithium-sulfur batteries, Chem. Rev. 114 (**2014**) 11751-11787.

[8] G. Zhou, E. Paek, G. S. Hwang, A. Manthiram, High-performance lithium-sulfur batteries with a self-supported, 3D $Li_2S$-doped graphene aerogel cathodes, Adv. Energy Mater. 6 (**2016**) 1501355.

[9] M. D. Walle, K. Zeng, M. Y. Zhang, Y. J. Li, Y. N. Liu, Flower-like molybdenum disulfide/carbon nanotubes composites for high sulfur utilization and high-performance lithium-sulfur battery cathodes, Appl. Surf. Sci. 473 (**2019**) 540-547.

[10] C. Tang, Q. Zhang, M. Q. Zhao, J. Q. Huang, X. B. Cheng, G. L. Tian, H. J. Peng, F. Wei, Nitrogen-doped aligned carbon nanotube/graphene sandwiches: Facile catalytic growth on bifunctional natural catalysts and their applications as scaffolds for high-rate lithium-sulfur batteries, Adv. Mater. 26 (**2014)** 6100-6109.

[11] W. H. Bin, W. Shuya, Z. Lei, R. Xu, H. H. Hing, X. W. Lou, Embedding sulfur in MOF-derived microporous carbon polyhedrons for lithium-sulfur batteries, Chem. Eur.

J. 19 (**2013)** 10804-10808.

[12] J. Q. Huang, X. F. Liu, Q. Zhang, C. M. Chen, M. Q. Zhao, S. M. Zhang, W. Zhu, W. Z. Qian, F. Wei, Entrapment of sulfur in hierarchical porous graphene for lithium–sulfur batteries with high rate performance from −40 to 60°C, Nano Energy 2 **(2013)** 314-321.

[13] H. J. Peng, J. Q. Huang, X. Y. Liu, X. B. Cheng, W. T. Xu, C. Z. Zhao, F. Wei, Q. Zhang, Healing high-loading sulfur electrodes with unprecedented long cycling life: spatial heterogeneity control, J. Am. Chem. Soc. 139 (**2017)** 8458-8466.

[14] S. Rehman, S. Guo, Y. Hou, Rational design of Si/$SiO_2$@hierarchical porous carbon spheres as efficient polysulfide reservoirs for high-performance Li-S battery, Adv. Mater. 28 (**2016)** 3167-3172.

[15] G. Zheng, Q. Zhang, J. J. Cha, Y. Yang, W. Y. Li, Z. W. She, Y. Cui, Amphiphilic surface modification of hollow carbon nanofibers for improved cycle life of lithium sulfur batteries, Electrochim. Acta 12 (**2018)** 641-649.

[16] Q. Li, J. Guo, J. Zhao, C. Wang, F. Yan, Porous nitrogen-doped carbon nanofibers assembled with nickel nanoparticles for lithium–sulfur batteries, Nanoscale 11 (**2019)** 647-655.

[17] L. F. Duan, L. J. Zhao, H. Cong, X. Y. Zhang, W. Lu, C. L. Xue, Plasma treatment for nitrogen-doped 3D graphene framework by a conductive matrix with sulfur for high-performance Li-S batteries, Small 15 (**2019)** 1804347.

[18] T. Zhou, W. Lv, J. Li, G. M. Zhou, Y. Zhao, S. X. Fan, B. L. Liu, B. H. Li, K. Y. Kang, Q. H. Yang, Twinborn $TiO_2$-TiN heterostructures enabling smooth trapping-diffusion-conversion of polysulfides towards ultralong life lithium-sulfur batteries, Energy Environ. Sci. 10 **(2017)** 1694-1703.

[19] S. Mei, C. Jafta, I. Lauermann, Q. Ran, M. Kargell, M. Ballauff, Y. Lu, Porous $Ti_4O_7$

particles with interconnected-pore structure as a high-efficiency polysulfide mediator for lithium–sulfur batteries, Adv. Funct. Mater. 27 (**2017)** 1701176.

[20] S. Liang, C. Liang, Y. Xia, H. Xu, H. Huang, X. Tao, Y. Gan, W. Zhang, Facile synthesis of porous $Li_2S$@C composites as cathode materials for lithium sulfur batteries, J. Power Sources 306 (**2016**) 200-207.

[21] K. Wang, G. Feng, C. Liang, Y. Xia, J. Zhang, Y. Gan, H. Huang, X. Tao, W. Zhang, Green and low-temperature synthesis of foam-like hierarchical porous carbon from $CO_2$ as superior lithium storage material, ACS Appl. Energy Mater. 1 (**2018**) 7123-7129.

[22] C. Liang, S. Liang, Y. Xia, Y. Chen, H. Huang, Y. Gan, X. Tao, J. Zhang, W. Zhang, $H_2O$-induced self-propagating synthesis of hierarchical porous carbon: a promising lithium storage material with superior rate capability and ultra-long cycling life, J. Mater. Chem. A 5 (**2017**) 18221-18229.

[23] C. Liang, S. Liang, Y. Xia, Y. Chen, H. Huang, Y. Gan, X. Tao, J. Zhang, W. Zhang, Synthesis of hierarchical porous carbon from metal carbonates towards high-performance lithium storage, Green Chem. 20 (**2018**) 1484-1490.

[24] C. Liang, L. Pan, S. Liang, Y. Xia, Z. Liang, Y. Gan, H. huang, J. Zhang, W. Zhang, Ultraefficient conversion of $CO_2$ into morphology-controlled nanocarbons: A sustainable strategy toward greenhouse gas utilization, Small 15 (**2019**) 1902249-1902256.

[25] M. Zhang, R. Hu, J. Liu, L. Ouyang, J. Liu, L. Yang, M. Zhu, A $ZnGeP_2$/C anode for lithium-ion and sodium-ion batteries, Electrochem. Common. 77 (**2017**) 85-88.

[26] M. Gao, X. Chen, H. Pan, L. Xiang, F. Wu, Y. Liu, Ultrafine $SnO_2$ dispersed carbon matrix composites derived by a sol-gel method as anode materials for lithium-ion batteries, Electrochim. Acta 55 (**2010**) 9067-9074.

[27] L. Z. Ouyang, Z. J. Cao, L. L. Li, H. Wang, J. W. Liu, D. Min, Y. W. Chen, F. M. Xiao, R. H. Tang, M. Zhu, Enhanced high-rate discharge properties of $La_{11.3}Mg_{6.0}Sm_{7.4}Ni_{61.0}Co_{7.2}Al_{7.1}$ with added graphene synthesized by plasma milling, Int. J. Hydrogen Energy 39 (**2014**) 12765-12772.

[28] C. Lin, L. Yang, L. Ouyang, J. Liu, H. Wang, M. Zhu, A new method for few-layer graphene preparation via plasma-assisted ball milling, J. Alloys Compd. 728 (**2017**) 578-584.

[29] L. Ouyang, L. Guo, W. Cai, J. Ye, R. Hu, J. Liu, J. Yang, M. Zhu, Facile synthesis of Ge@FLG composites by plasma assisted ball milling for lithium ion battery anodes, J. Mater. Chem. A 2 (**2014**) 11280-11285.

[30] L. Ouyang, Z. Cao, H. Wang, R. Hu, M. Zhu, Application of dielectric barrier discharge plasma-assisted milling in energy storage materials-A review, J. Alloys Compd. 691 (**2017**) 422-435.

[31] L. Ni, Z. Wu, G. Zhao G, C. Sun, C. Zhou, X. Gong, G. Diao, Core–shell structure and interaction mechanism of γ-$MnO_2$ coated sulfur for improved lithium-sulfur batteries, Small 13 (**2017**) 201603466.

[32] Y. Zhang, L. Wang, A. Zhang, Y. Song, X. Li, H. Feng, X. Wu, P. Du, Novel $V_2O_5$/S composite cathode material for the advanced secondary lithium batteries, Solid State Ionics 181 (**2010**) 835-838.

[33] Z. Liu, X. Zheng, S. L. Luo, S. Q. Xu, N. Y. Yuan, J. N. Ding, High performance Li–S battery based on amorphous $NiS_2$ as the host material for the S cathode, J. Mater. Chem. A 4 (**2016**) 13395-13399.

[34] X. Li, Y. Lu, Z. Hou, W. Zhang, Y. Zhu, Y. Qian, J. Liang, Y. Qian, $SnS_2$-compared to $SnO_2$-stabilized S/C composites toward high-performance lithium sulfur batteries, ACS Appl. Mater. Interfaces 8 (**2016)** 19550-19557.

[35] X. Zhou, X. Ma, C. Ding, W. Meng, S. Xu, L. Chen, D. Duan, S. Liu, A 3D stable and highly conductive scaffold with carbon nanotubes/carbon fiber as electrode for lithium sulfur batteries, Mater. Lett. 251 (**2019**) 180-183.

[36] S. Jiang, M. Chen, X. Wang, P. Zeng, Y. F. Li, H. Liu, X. Li, C. Huang, H. Shu, Z. Luo, C. Wu, A tin disulfide nanosheet wrapped with interconnected carbon nanotube networks for application of lithium-sulfur batteries, Electrochim. Acta 313 (**2019**) 151-160.

[37] Z. W. Seh, Y. Sun, Q. Zhang, Y. Cui, Designing high-energy lithium-sulfur batteries, Chem. Soc. Rev. 45 (**2016**) 5605-5634.

[38] A. Rosenman, E. Markevich, G. Salitra, D. Aurbach, A. Garsuch, F. Chesneau, Review on Li-Sulfur battery systems: an integral perspective, Adv. Energy Mater. 5 (**2015**) 1500212.

[39] R. Xu, J. Lu, K. Amine, Progress in mechanistic understanding and characterization techniques of Li-S batteries, Adv. Energy Mater. 5 (**2015**) 1500408.

[40] C. Dai, J. M. Lim, M. Wang, L. Hu, Y. Chen, Z. Chen, H. Chen, S. J. Bao, B. Shen, Y. Li, G. Henkelman, M. Xu, Honeycomb-Like Spherical Cathode Host Constructed from Hollow Metallic and Polar $Co_9S_8$ Tubules for Advanced Lithium-Sulfur Batteries, Adv. Funct. Mater. 28 (**2018**) 1704443.

[41] J. Wei, H. Su, C. Qin, B. Chen, H. Zhang, J. Wang, Multifunctional $Co_9S_8$ nanotubes for high-performance lithium-sulfur batteries, J. Electroanal. Chem. 837 (**2019**) 184-190.

[42] H. Zhang, Z. B. Zhao, Y. N. Hou, Y. C. Tang, J. J. Liang, X. G. Liu, Z. C. Zhang, X. Z. Wang, J. S. Qiu, Highly stable lithium-sulfur batteries based on p-n heterojunctions embedded on hollow sheath carbon propelling polysulfides conversion, J. Mater. Chem. A 7 (**2019**) 9230-9240.

[43] N. Wang, B. Chen, K. Qin, E. Liu, C. Shi, C. He, N. Zhao, Rational design of $Co_9S_8$/CoO heterostructures with well-defined interfaces for lithium sulfur batteries: A study of synergistic adsorption-electrocatalysis function, Nano Energy 60 (**2019**) 332-339.

[44] J. Zhou, X. Liu, J. Zhou, H. Zhao, N. Lin, L. Zhu, Y. Zhu, G. Wang, Y. Qian, Fully integrated hierarchical double-shelled $Co_9S_8$@CNT nanostructures with unprecedented performance for Li–S batteries, Nanoscale Horiz. 4 (**2019**) 182-189.

[45] T. Meng, J. Gao, Y. Liu, J. Zhu, H. Zhang, L. Ma, M. Xu, C.M. Li, J. Jiang, Highly Puffed $Co_9S_8$/Carbon Nanofibers: A Functionalized S Carrier for Superior Li-S Batteries, ACS Appl. Mater. Interfaces 11 (**2019**) 26798-26806.

[46] W. Lin, G. He, Y. Huang, X. Chen, 3D hybrid of $Co_9S_8$ and N-doped carbon hollow spheres as effective hosts for Li-S batteries, Nanotechnology 31 (**2020**) 035404.

[47] M. D. Walle, Z. F. Zhang, M. Y. Zhang, X. L. You, Y. J. Li, Y. N. Liu, Hierarchical 3D nitrogen and phosphorous codoped graphene/carbon nanotubes-sulfur composite with synergistic effect for high performance of lithium-sulfur batteries, J. Mater. Sci. 53 (**2018**) 2685-2696.

[48] S. Liang, Y. Xia, C. Liang, Y. Gan, J. Zhang, X. Tao, W. Sun, W. Han, W. Zhang, A green and facile strategy for the low-temperature rapid synthesis of $Li_2S$@PC-CNT cathodes with high $Li_2S$ content in advanced Li-S batteries, J. Mater. Chem. A 6 (**2018**) 9906-9914.

[49] W. Tong, Y. Huang, W. Jia, X. C. Wang, Y. Guo, Z. Sun, D. Jia, J. Zong, Leaf-like interconnected network structure of MWCNT/$Co_9S_8$/S for lithium-sulfur batteries, J. Alloys Compd. 731 (**2017**) 964-970.

[50] T. Chen, B. Cheng, R. Chen, Y. Hu, G. Zhu, Y. Wang, J. Liang, Z. Tie, J. Liu, Z. Jin, Metallic and polar $Co_9S_8$ inlaid carbon hollow nanopolyhedra as efficient polysulfide

mediator for lithium-sulfur batteries, Nano Energy 38 (**2017)** 239-248.

[51] S. Zhao, X. Tian, Y. Zhou, B. Ma, N. Angulakshmi, Three-dimensionally interconnected $Co_9S_8$/MWCNTs composite cathode host for lithium-sulfur batteries, J. Energy Chem. 46 (**2020**) 22-29.

[52] Q. Pang, D. Kundu, L. F. Nazar, A graphene-like metallic cathode host for long-life and high-loading lithium-sulfur batteries, Mater. Horiz. 3 (**2016**) 130-136.

[53] C. Dai, J. M. Lim, M. Wang, L. Hu, Y. Chen, Z. Chen, H. Chen, S. J. Bao, B. Shen, Y. Li, G. Henkelman, M. Xu, Honeycomb-like spherical cathode host constructed from hollow metallic and polar $Co_9S_8$ tubules for advanced lithium-sulfur batteries, Adv. Funct. Mater. 28 (**2018**) 1704443.

[54] T. Chen, L. Ma, B. Cheng, R. Chen, Y. Hu, G. Zhu, Y. Wang, J. Liang, Z. Tie, J. Liu, Z. Jin, Metallic and polar $Co_9S_8$ inlaid carbon hollow nanopolyhedra as efficient polysulfide mediator for lithium-sulfur batteries, Nano Energy 38 (**2017**) 239-248.

[55] Y. L. Zhou, D. Yan, H. Y. Xu, J. K. Feng, X. L. Jiang, J. Yue, J. Yang, Y. T. Qian, Hollow nanospheres of mesoporous $Co_9S_8$ as a high-capacity and long-life anode for advanced lithium ion batteries, Nano Energy 12 (**2015**) 528-537.

[56] X. Life, C. Yuliang, X. Jie, B. Schwenzer, M. H. Engelhard, L. V. Saraf, Z. M. Nie, G. J. Exarhos, J. Liu, A soft approach to encapsulate sulfur: polyaniline nanotubes for lithium-sulfur batteries with long cycle life, Adv. Mater. 24 (**2012)** 1176-1181.

[57] X. Pu, G. Yang, C. Yu, Liquid-type cathode enabled by 3D sponge-like carbon nanotubes for high energy density and long cycling life of Li-S batteries, Adv. Mater. 26 (**2014**) 7456-7461.

[58] C. Dai, J. M. Lim, M. Wang, L. Hu, Y. Chen, Z. Chen, H. Chen, S. Bao, B. Shen, L. Li, G. Henkelman, M. Xu, Honeycomb-like spherical cathode host constructed from

hollow metallic and polar $Co_9S_8$ tubules for advanced lithium-sulfur batteries, Adv. Fun. Mater. 28 (**2018**) 1704443.

[59] J. He, Y. Chen, A. Manthiram, MOF-derived cobalt sulfide grown on 3D graphene foam as an efficient sulfur host for long-life lithium-sulfur batteries, iScience 4 (**2018**) 36-43.

[60] W. Qian, Q. Gao, H. Zhang, W. Tian, Z. Li, Y. Tan, Cross-linked polypyrrole grafted reduced graphene oxide-sulfur nanocomposite cathode for high performance Li-S battery, Electrochim. Acta 235 (**2017)** 32-41.

[61] L. Fan, H. Wu, X. Wu, M. Wang, J. Cheng, N. Zhang, Y. Feng, K. Sun, Fe-MOF derived jujube pit like $Fe_3O_4$/C composite as sulfur host for lithium-sulfur batteries, Electrochim. Acta 295 (**2019**) 444-451.

[62] T. Ma, M. Liu, T. Huang, A. Yu, $Al_2O_3$-doped ZnO coating of carbon nanotubes as cathode material for lithium-sulfur batteries, J. Power Sources 398 (**2018**) 75-82.

[63] J. Wu, S. Li, P. Yang, H. Zhang, C. Du, J. Xu, X. Song, S@$TiO_2$ nanospheres loaded on PPy matrix for enhanced lithium sulfur batteries, J. Alloys Compd. 783 **(2018)** 279-285.

[64] M. Qi, X. Liang, F. Wang, M. Han, J. Yin, M. Chen, Sulfur-impregnated disordered $SnO_2$/carbon aerogel core-shell microspheres cathode for lithium-sulfur batteries, J. Alloys Compd. 799 (**2019**) 345-350.

[65] Z. W. Seh, J. H. Yu, W. Li, P. C. Hsu, H. T. Wang, Y. M. Sun, H. B. Yao, Q. F. Zhang, Y. Cui, Two-dimensional layered transition metal disulphides for effective encapsulation of high-capacity lithium sulphide cathodes, Nat. Commun. 5 (**2014**) 5017.

[66] Z. Li, J. T. Zhang, B. Y. Guan, D. Wang, L. M. Liu, X. W. Lou, A sulfur host based on titanium monoxide@carbon hollow spheres for advanced lithium-sulfur batteries, Nat. Commun. 7 (**2016**) 13065.

[67] J. Huang, X. Tang, K. Liu, Z. Li, Synthesis of porous carbon-coated polycrystalline $Co_9S_8$ for long-term lithium ion battery, Mater. Lett. 210 (**2018**) 88-91.

[68] H. Zhou, J. Hu, Facile synthesis of multi-walled carbon nanotubes/$Co_9S_8$ composites with enhanced performances for sodium-ion battery, Mater. Lett. 195 (**2017**) 26-30.

[69] C. Yong, X. L. Li, M. S. Zheng, M. P. Yang, X. L. Yang, Q. F. Dong, Ultra-high rates and reversible capacity of Li-S battery with a nitrogen-doping conductive Lewis-Base matrix, Electrochim. Acta 192 (**2016**) 467-474.

[70] Y. Huang, M. Zhong, F. Shi, X. Liu, Z. Tang, Y. Wang, Y. Huang, H. Hou, X. Xie, C. Zhi, An intrinsically stretchable and compressible supercapacitor containing a polyacrylamide hydrogel electrolyte, Angew. Chem. 56 (**2017**) 9141-9145.

[71] L. Yuan, X. Qiu, L. Chen, W. Zhu, New insight into the discharge process of sulfur cathode by electrochemical impedance spectroscopy, J. Power Sources 189 (**2009**) 127-132.

[72] T. Chen, Z. Zhang, B. Cheng, R. chen, Y. Hu, L. Ma, J. Liu, Z. Jin, Self-templated formation of interlaced carbon nanotubes threaded hollow $Co_3S_4$ nanoboxes for high-rate and heat-resistant lithium-sulfur batteries, J. Am. Chem. Soc. 139 (**2017**) 12710-12715.

[73] M. Zheng, Y. Chi, H. Tang, X. Jiang, L. Zhang, S. Zhang, H. Pang, Q. Xu, Carbon nanotube-based materials for lithium-sulfur batteries, J. Mater. Chem. A 7 (**2019**) 17204-17241.

[74] Y. J. Li, J. M. Fan, M. S. Zheng, Q. F. Dong, A novel synergistic composite with multi-functional effects for high-performance Li-S batteries, Energ. Environ. Sci. 9 (**2016**) 1998-2004.

[75] S. Cheng, X. Xia, H. Liu, Y. Chen, Core-shell structured $MoS_2$@S spherical cathode

with improved electrochemical performance for lithium-sulfur batteries, J. Mater. Sci. Technol. 34 (**2018)** 1912-1918.

[76] Z. Guo, H. Nie, Z. Yang, W. Hua, C. Ruan, D. Chen, S. Huang, Lithium–sulfur batteries: 3D CNTs/graphene-S-$Al_3Ni_2$ cathodes for high-sulfur-loading and long-life lithium–sulfur batteries, Adv. Sci. 5 (**2018**) 1800026.